https://doi.org/10.1590/jatm.v15.1304 ORIGINAL PAPER

Performance Enhancement of a Solar Air Collector Using a V-Corrugated Absorber

Angham Fadil Abed[1], Ruaa Braz Dahham[2], Noora Abdul Wahid Hashim[1,*], Raisan Faris Hamad[1]

1. University of Kufa – Engineering Faculty – Mechanical Engineering Department – Najaf – Iraq.
2. Directorate General of Education – Kufa/Najaf – Iraq.

*Correspondence author: nooraa.alkhalidi@uokufa.edu.iq

ABSTRACT

Solar energy is one of the most efficient forms of renewable energy. Solar air collectors are promising utilization of solar energy. The present study used unsteady three-dimensional Computational Fluid Dynamic (CFD) analysis to investigate the heat transfer and fluid friction in solar air collectors with smooth and v-corrugation absorber plates. The studied parameters are Reynolds number, v-corrugation height, and pitch. Three Reynolds number (500, 1000, 1500) values were used with three arrangements configuration of the v-corrugation of relative heights of 0.10, 0.16, and 0.23. Roughness pitches varied between 1.33, 1.66, and 2. By comparing the simulated thermal efficiency with the currently known experimental values, great agreement can be approved. Results show the superiority of the performance of v-corrugated collector against the traditional or smooth type. The outlet temperature obtained in case of relative roughness height = 0.23 and relative roughness pitch = 2 is 61 °C, while it is 53 °C for a smooth type. Also, a higher thermal efficiency of 46.7 % can be obtained compared to 33.01% for smooth type.

Keywords: Nusselt number; Solar air collector; CFD; Friction factor; Thermal efficiency.

INTRODUCTION

Every day, energy demand grows. There are many distinct types of energy resources, including major and minor, renewable and non-renewable, commercial and non-commercial energies. Solar energy is one of the most practical forms of renewable energy. It has been regarded as a large and cost-effective energy source due to its abundance. Also it can be harnessed after years of research. Solar air collector systems were created with the primary goal of gathering as much heat energy as possible while reducing pumping costs. In order to decrease the consumption of oil, gas, electricity, and other equivalent sources of heat, several different forms of solar heating systems have been devised (Kumar *et al.* 2017).

One of the most promising uses for air solar collectors is providing hot air for drying agricultural and marine products, or air conditioning processes especially in winter. In these devices, solar energy is converted to heat which is transferred to air. The most prevalent solar collectors used for domestic water heating are the flat-plate collectors. Compared to solar water collectors, air collectors are less expensive and require less maintenance. A traditional flat-plate collector is a metal box insulated with a plastic or glass lid (termed as the glazing) with an absorber of dark color. Lower than 80 °C temperatures can be used to heat liquids or air. Traditional collectors have a lower thermal efficiency because of low heat transfer convective coefficient

Received: Apr 04, 2023 | **Accepted:** May 22, 2023
Section editor: Paulo Greco
Peer Review History: Single Blind Peer Review.

through the absorber and the moving air stream (Amraoui and Aliane 2018; Yadav and Bhagoria 2013). By adding baffles or other impediments to the absorber surface of the collectors, altering number of covers and passes of flow, dual glassing, or making corrugation in the absorber, the system's thermal performance can be enhanced. As a result, the absorber and the coefficients of air heat transfer will be higher (Hakam *et al.* 2016; Hedayatizadeh *et al.* 2016). Numerous researches have focused into the impact of various roughness geometries of absorber on heat transfer. Numerical research of solar sloped collectors was carried out by Varol and Oztop (2007). The results showed that transfer of heat increased with increasing aspect ratio and Rayleigh number but decreased when length of wave increased. Chaube *et al.* (2006) employed CFD to predict the improvement of heat transfer and characteristics of flow based on the rib-roughed absorber surface of a 2D air solar heater. Karmare and Tikekar (2010) used Ansys Fluent to optimize numerically the geometric design of various metal rib shapes for heat transmission of an absorber in air solar heater. The rib height and width of 2 mm, relative width gap of 1, relative pitch gap of 0.25, and *Re* ranging from (3000 to 18, 000) in rectangular air solar heater. Heat transfer improvement carried on by inclined gap with continuous rib arrangement was investigated by Aharwal *et al.* (2008). They found that the friction factor and Nusselt number increased by 2.2-2.87 and 1.48-2.59 times, respectively, compared with smooth collectors. Karmare and Tikekar (2010) utilized CFD to quickly and economically assess flow of fluid and transmission of heat in air solar heaters. A collection plate with 600 ribs in the forms of circles, squares, and triangles was used in their experiment. The direction of the airflow was inclined. On the surface, the ribs were staggered out in a specified grid. The ribs maximized heat transfer due to their square cross-section and 58^0 angle of attack. When a square plate was utilized instead of one with a smooth surface, heat transmission is improved by 30%. Chaichan *et al.* (2016) raised the temperature of the surrounding air by nearly 101 percent using an aluminum flat plate installed in a 1 m^2 opaque heater Solar Air Collector (SAC). The stream of air entered from top and exited from bottom of the collector. The researchers showed that by absorbing heat from solar radiation, an aluminum absorber may be used as a heating source which was essential to augment the thermal performance of the solar heater. Darici and Kilic (2020) combined two SAC, an absorber corrugate in the form of trapezoidal and another flat absorber. They examined how SAC thermal efficiency was impacted by the absorber form and air mass flow rate. There were used three rate values of mass flow for air: 0.022, 0.033, and 0.044 kg/s. Results indicated that when the rate of mass flow was reduced, SAC output temperature increased. The highest difference of temperature in the SAC with a trapezoidal absorber was about 9 °C greater than in flat absorber at a mass rate of 0.022 kg/s. SAC thermal performance increased as the rate of mass flow increased when employing the trapezoidal absorber plate at 0.044 kg/s, with a daily average thermal efficiency about 63%. Zheng *et al.* (2017) created mathematical models to evaluate the thermal performance of corrugated model SAC in cold-climate environments. In contrast to the temperature of the input air and the width of the corrugated plate, the collector thermal efficiency decreased as the corrugation height, surface area, intensity of radiation, velocity of air, and temperature of ambient were increased. Both exegetical and thermal efficiency attained 73 percent. Manjunath *et al.* (2018) used a CFD analysis for a SAC with sinusoidal shape absorber. The values of Re used were 4,000 to 24,000. In comparison to a typical air solar collector with a smooth plate, their studies showed that sinusoidal waves greatly increased heat transmission and improved flow disturbances, leading to an increase in average thermal efficiency by 12.5%. To enhance thermal performance in a solar heat exchanger duct, Promvonge *et al.* (2022) tested a newly developed louver-punched V-baffle (LPVB) vortex generator analytically and experimentally. Air was employed in the test fluid, flowing through the continuously heated duct at Reynolds numbers (*Re*) ranging from 5,300 to 23,000. According to their research, the LPVB with PR (relative baffle pitches) = 1.5, (louver angle) = 45°, and LR (relative louver size) = 0.9 performs at its best. Two semi-cylinders, two flexible baffles, and alternately attached lower and upper channel walls were used in Salih *et al.* (2023) study of a forced fluid flowing inside a horizontal channel. The semi-cylinders, which are heated by constant temperature, are filled with a phase-change substance. While the pressure drop throughout the channel significantly diminishes, the Nusselt number is only marginally (0.9%) increased by the flexible baffles with a lower modulus of elasticity.

Based on the previous survey of the literature, it appears that relatively little researches employed a 3D transient numerical studies analysis with variable climatic conditions of artificially roughened SAC having an absorber in the form of v-corrugated plate, which makes the present work novel. Using a unique CFD analysis, the current work intends to fill a knowledge gap by systematically analyzing the unsteady, 3D flow and influence of v-corrugated absorber on heat transmission and fluid friction

in SAC. Additionally, this work examines the change of meteorological factors, including solar radiation, temperature of environment, wind velocity, and temperature of inlet air, and how these parameters affected the effectiveness of various solar air collectors' arrangement (smooth absorber plate SAC and v-corrugated absorber plate SAC). This study's main objective is to find out how air solar collectors' average Nusselt number, average friction factor, and thermal performance are influenced by factors like *Re*, relative roughness height (*e/H*), and relative roughness pitch (*p/H*) of absorber plates. In order to establish a parametric investigation, a v-corrugated absorber plate SAC was compared to a smooth flat plate SAC using COMSOL SOFTWARE V5.5.

MODEL DESCRIPTION

A schematic of the three-dimensional SACs are displayed in Fig. 1, which has a conventional flat plate SAC (smooth absorber plate SAC). A collection of equal-sided triangles makes up the v-corrugated plate geometry. The SAC is a box of metal with a bottom made of dark-colored aluminum absorber plates, a top made of extremely transparent, anti-reflective glass called glazing, and a space between them. The bottom surface of the absorber is insulated by using a glass wool layer to prevent losses of heat. Air temperature rises as a result of heat transfer of the absorber caused by solar radiation that penetrates the glassing layer, falls on the absorber, and causes increase in temperature. The collector length and width are 1.2 m, 0.3 m, respectively. The other geometric specifications for the present SAC are shown in Table 1. CFD simulations are conducted using various collections of height (e), pitch (p), and *Re*. Each configuration of collectors is examined at three distinct values of *Re* ranging (500, 1000, 1500) corresponding to rates of mass flow (0.0014, 0.0029, 0.0044 kg/s).

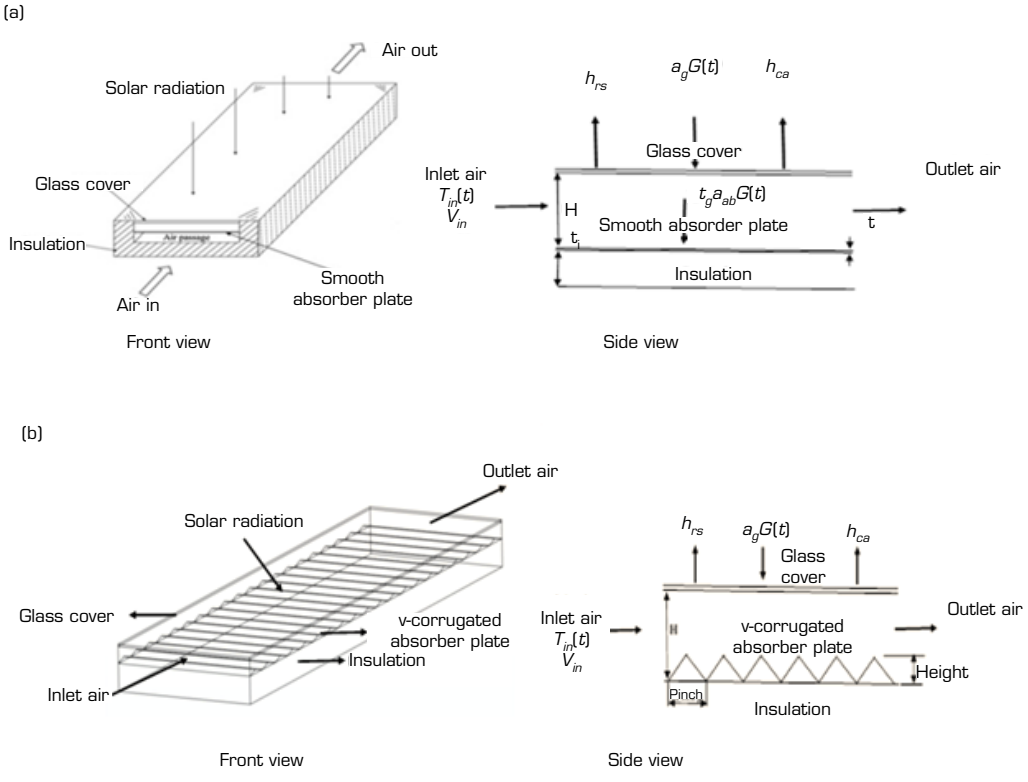

Source: Elaborated by the authors.

Figure 1. Thermal schematics of the solar air collectors. (a) Smooth absorber SAC; (b) V-corrugated absorber SAC.

Table 1. Criteria for solar air collectors' geometry.

Parameter	Value	Parameter	Value
Absorber plate thickness, t (m)	0.001	e(m)	0.003, 0.005, 0.007
Duct height H (m)	0.03	p(mm)	0.04, 0.05, 0.06
Insulation thickness, t_i (m)	0.01	e/H	0.10, 0.16, 0.23
Glass layer thickness (m)	0.004	p/H	1.33, 1.66, 2
Hydraulic diameter, D_h (m)	0.05454		

Source: Elaborated by the authors.

NUMERICAL ANALYSIS

CFD Setup and Boundary Conditions

The present study used a model by COMSOL SOFTWARE V.5.5. This software is a robust interactive environment that is used to model and solve science and engineering problems of all kinds. With this program, a conventional model for one form of physics can be extended easily to Multiphysics models that simultaneously solve combined physics phenomena. Incompressible three-dimensional transient laminar flow model is considered. The flow is taken as laminar because of low values of inlet air velocity, which depend on ambient speed that ranges from 0.1-0.4 m/s. In contrast to air, whose thermal characteristics vary with temperature, the absorber plate, insulation, and transparent cover all have fixed thermal properties. The convergence limit of relative deviations of continuity, velocity components, and energy are assumed to be, 10^{-3}, 10^{-3}, and 10^{-6} respectively. The creation of the studied geometry is the initial stage in CFD analysis. A further step is to create a mesh. The input variables are solar radiation G ambient temperature T_a, inlet temperature T_{in} and wind velocity V_w. The various boundary conditions can be written as follows for both configurations (Fig. 1a and b): At inlet: variable inlet air temperature T_{in} (t) is taken. Velocity of air is considered uniform at inlet. Re is used to determine the average inlet velocity. At the top clear glass cover, solar radiation flux is applied and will changes during the simulated day, and the outer exchanges from the transparent cover to outside air are convective equal to (hca($T_g - T_a$)) and radiative equal to ($h_{rs}(T_g - T_s)$). The glass cover's transmittance value is 0.9. Heat flux equals to ($\tau_g\, a_{ab}\, G(t)$) be applied in upper absorber surface. Aluminum plate heat absorption coefficient is 95 percent, at the lateral and bottom plates, which are designated as a "adiabatic wall" because they are thought to be a good insulation. No-slip condition is applied on all walls. At the channel's outlet, pressure is assumed equal to 101325 Pa. Sky temperature, T_S is calculated by the formula used by Winbank (1963) (Eq. 1):

$$T_s = 0.0552 T_a^{1.5} \tag{1}$$

Governing Equations

The unsteady incompressible laminar flow in a smooth and v-corrugated plate SAC is governed by the continuity, momentum, and energy equations. The following is a description of the governing equations for three-dimensional transient CFD simulations (Hassan 2022).

Continuity equation (Eq. 2):

$$\frac{\partial \rho}{\partial t} + \frac{\partial u}{\partial x} + \frac{\partial v}{\partial y} + \frac{\partial w}{\partial z} = 0 \tag{2}$$

Momentum equations (Eqs. 3–5) (Hassan 2022):

$$\rho\left(\frac{\partial u}{\partial t}+u\frac{\partial u}{\partial x}+v\frac{\partial u}{\partial y}+w\frac{\partial u}{\partial z}\right)=\rho g_x-\frac{\partial P}{\partial x}+\mu\left(\frac{\partial^2 u}{\partial x^2}+\frac{\partial^2 u}{\partial y^2}+\frac{\partial^2 u}{\partial z^2}\right) \tag{3}$$

$$\rho\left(\frac{\partial v}{\partial t}+u\frac{\partial v}{\partial x}+v\frac{\partial v}{\partial y}+w\frac{\partial v}{\partial z}\right)=\rho g_y-\frac{\partial P}{\partial y}+\mu\left(\frac{\partial^2 v}{\partial x^2}+\frac{\partial^2 v}{\partial y^2}+\frac{\partial^2 v}{\partial z^2}\right) \tag{4}$$

$$\rho\left(\frac{\partial w}{\partial t}+u\frac{\partial w}{\partial x}+v\frac{\partial w}{\partial y}+w\frac{\partial w}{\partial z}\right)=\rho g_z-\frac{\partial P}{\partial z}+\mu\left(\frac{\partial^2 w}{\partial x^2}+\frac{\partial^2 w}{\partial y^2}+\frac{\partial^2 w}{\partial z^2}\right) \tag{5}$$

Energy equation (Eq. 6) (Hassan 2022):

$$\rho C_p\left(\frac{\partial T}{\partial t}+\frac{\partial T}{\partial t}+u\frac{\partial T}{\partial x}+v\frac{\partial T}{\partial y}+w\frac{\partial T}{\partial z}\right)=K\left(\frac{\partial^2 T}{\partial x^2}+\frac{\partial^2 T}{\partial y^2}+\frac{\partial^2 T}{\partial z^2}\right) \tag{6}$$

Data Reduction and Grid Independence

In the current CFD model, the average Nusselt number (*Nu*) , average friction factor (*Cf*) and average thermal efficiency (η_{th}) in a smooth and v-corrugation absorber SAC are the primary research interests. For solar air collectors, the average Nu is calculated by Eq. 7 (Choi H and Choi K 2020; Rouissi *et al.* 2021; Yadav and Bhagoria 2013):

$$Nu=\frac{hD_h}{K} \tag{7}$$

Cf for a SACs (smooth and v-corrugation absorber) is computed by Eq. 8 (Choi H and Choi K 2020; Hassan 2022; Yadav and Bhagoria 2013):

$$Cf=\frac{(\Delta P/l)D_h}{2\rho v^2} \tag{8}$$

The percentage between the thermal power that is actually transferred to air and the maximum theoretical power is referred to as the thermal efficiency of SAC and can be written by Eq. 9 (Rouissi *et al.* 2021):

$$\eta_{th}=\frac{Q_u}{Q_{max}} \tag{9}$$

where (Eq. 10 and 11):

$$Q_u=\dot{m}C_p\Delta T \tag{10}$$

$$Q_{max}=G(t)S \tag{11}$$

The numerical domain has been discretized using elements in three dimensions. A finer meshing at v-roughened has been done to be able to carefully investigate the flow characteristic and heat transmission in corrugated zones. Table 2 shows the characteristics of the tested meshes. As seen in Fig. 2, coarser mesh has been employed in various places. Near the heating wall, the boundary layers are fastened together. A test of grid independence has been performed in order to reduce computation time while maintaining the precision of the meshes, which is important for the quality of the findings. This test for the average output air temperature of v-corrugated SAC and smooth SAC is shown in Fig. 2b. As a result, the mesh refinement findings show a difference between two sets of data that is less than 2%. Further refining has an impact on the output, but does not alter it by more than 1.25 percent, therefore this mesh quality is considered suitable for calculation.

Table 2. Characteristics of the tested meshes.

	Mesh size	Domain elements		Boundary elements		Edge elements	
		Smooth SAC	v-corrugated SAC	Smooth SAC	v-corrugated SAC	Smooth SAC	v-corrugated SAC
1	Grid 1	50895	56502	12118	14044	770	1653
2	Grid 2	104001	104541	18548	20796	952	2001
3	Grid 3	234064	256391	35453	40006	1289	2804
4	Grid 4	1410114	1438827	141538	150400	2505	5603
5	Grid 5	3649021	10220004	267562	629000	3423	11783

Source: Elaborated by the authors.

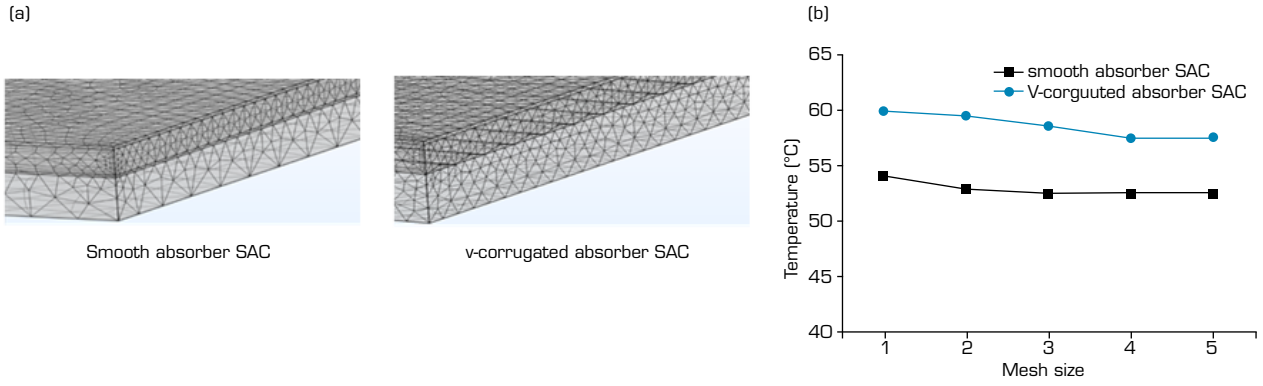

Source: Elaborated by the authors.

Figure 2. (a) Mesh of the solar collectors; (b) Grid independency test for outlet air temperature.

Properties of Air

Air's thermophysical parameters are influenced by pressure, temperature, and humidity. The following thermophysical properties, which hold true for temperature ranges between 280 and 470 K, will be incorporated into the present model for the accuracy of the simulation results (Eqs. 12–15) (Rouissi *et al.* 2021):

$$\rho = 3.9147 - 0.016082T + 2.9013 \times 10^{-5}T^2 - 1.9407 \times 10^{-5}T^3 \quad (12)$$

$$\mu = (1.6157 + 0.06523T - 3.0297 \times 10^{-5}T^2) \times 10^{-6} \quad (13)$$

$$K = (0.0015215 + 0.097459T - 3.3322 \times 10^{-5}T^2) \times 10^{-3} \quad (14)$$

$$C_p = 1009.26 - 0.0040403T + 0.00061759T^2 - 0.0000004097T^3 \quad (15)$$

RESULTS AND DISCUSSIONS

Numerical Results Validation

Thermal efficiency of the smooth absorber SAC is compared with experimental findings provided by Hameed *et al.* (2021) in order to confirm the CFD outcomes obtained in this work at various air flow rates, as seen in Fig. 3. In the present model, the

used climatic variables such as solar radiation, ambient temperature and wind velocity, are the as in experimental investigation of Hameed *et al.* (2021) for this validation setup in order to assess and contrast the system's energy performance. The average absolute difference between the experimental and estimated values of thermal efficiency is 6.44 percent.

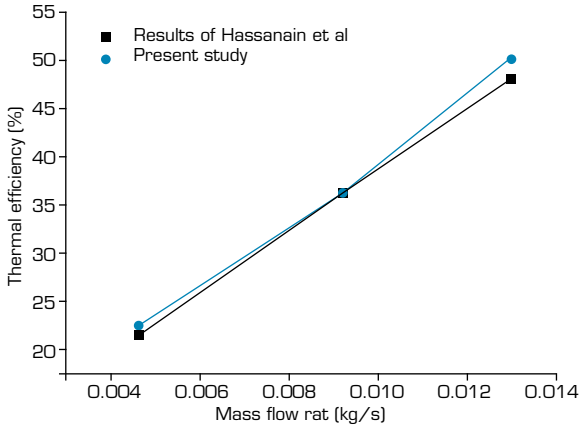

Source: Elaborated by the authors.

Figure 3. Average thermal efficiency variation with mass flow rate: a comparison of the experimental research of Hameed *et al.* (2021) and present work.

Weather Conditions

The numerical simulation was run on a sunny September day (2/9/2019) at Kufa, Iraq, using experimental climatic data. On a sunny day, the solar radiation intensity peaks between 12:00 and 13:00 and exceeds 1000 W/m^2. The outside temperature and wind speed were 40 to 49.7 0C and 0.1 to 0.4 m/s, respectively.

Velocity and Temperature Distribution

Figure 4 displays the plots of the temperature distribution contour for the two SAC types (smooth and v-corrugated) at various periods at (*Re* 1500). As air moves over the hot absorber surface, heat is transmitted to air, and the temperature of moving fluid slowly rises with distance along the duct. As can be seen at 15 p.m. the corrugation in the absorber causes the highest temperature (102°C) in the corrugated collector, but it is 95°C in the smooth, indicating an improvement in the recommended collector. Due to modeling, when using thermal storage of an absorbing plate, the temperature in two collectors is low in the morning (9 a.m.) and starts to rise to high values at around 3 p.m. (the same trend is shown in Naraghi and Blanchard (2015)).

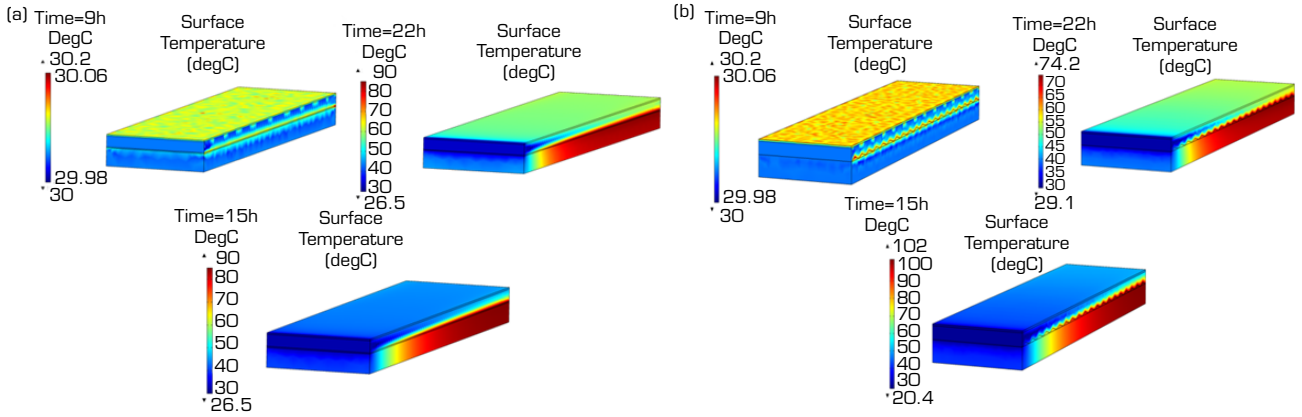

Source: Elaborated by the authors.

Figure 4. Temperature distribution for the two collectors. (a) *Re* = 1500 Smooth absorber solar air collector; (b) *Re* = 1500, *e/H* = 0.23 V-corrugated absorber solar air collector.

Figure 5 shows the streamlines and velocity distribution for the smooth and corrugated absorber solar air collectors at values of (e/H = 0.23) and various values of periods for (Re = 1500). Because the flow is expected to be laminar and the velocity increases at the corrugated collector rather than the smooth collector, the airflow is nearly uniform inside the two collectors. The velocity profiles are not comparable, and a corrugated absorber is found to have a higher velocity at a rate of around 1.5 times the inlet velocity. As the sun radiation increased, the magnitude of the velocity increased.

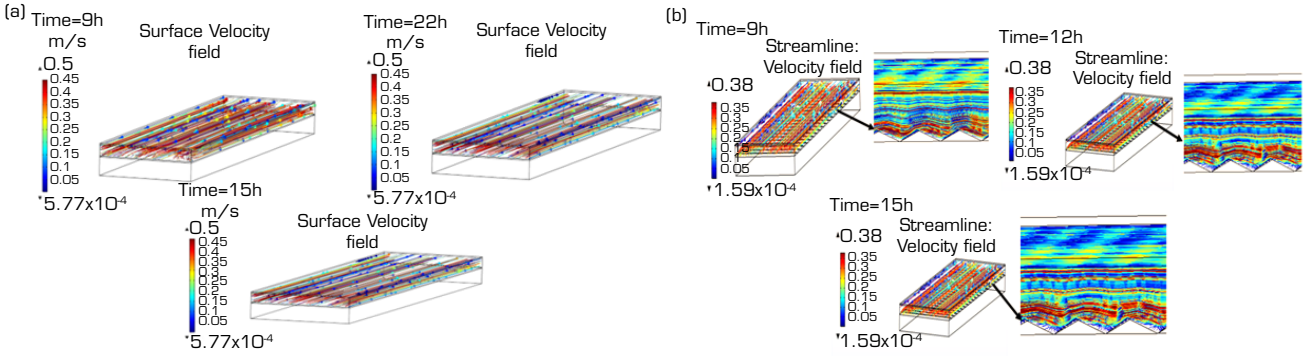

Source: Elaborated by the authors.

Figure 5. Streamlines and velocity distribution for the two collectors. (a) Re = 1500 smooth absorber solar air collector; (b) Re = 1500, e/H = 0.23 v- corrugated absorber solar air collector.

Heat transfer

Figure 6 compares a smooth absorber SAC with a v-corrugated absorber SAC using average Nusselt number and average output air temperature values for various (e/H) and (p/H) as function of Reynolds number. Because the v-corrugation increases local velocity, the corrugation in the absorber can produce better heat transfer performance than a smooth plate. The results show as Re rises, the average Nu also rises, which improves the transfer rate of heat. For constant values of (p/H) and Re, the average Nu grows when (e/H) increases. This is because, at a given amount of Reynolds number, the local air velocity increases more rapidly as the height (e/H) increases, leading to improved heat transfer performance. It is also evident from the data given, at a fixed value of (e/H) and Re, the average Nu rises as the (p/H) drops. The number of corrugations rises when pitch (p/H) decreases. The flow acceleration area expands as the number of corrugations rises, as a result the average Nu increases. The inclusion of v-corrugation in the absorber enhances the collector area as compared to a smooth duct and a rise in temperature of the outlet air occurs.

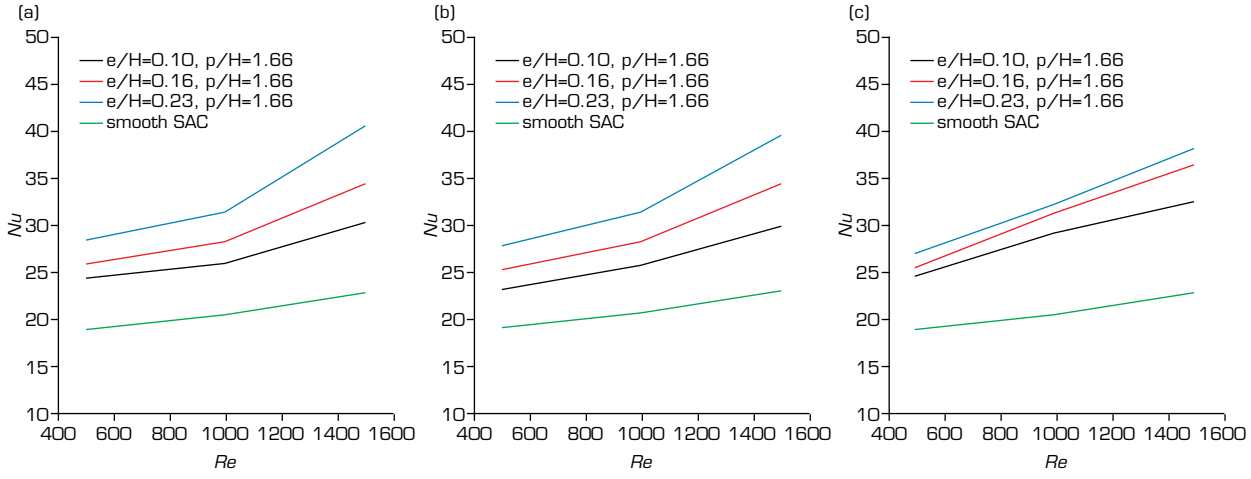

Source: Elaborated by the authors.

Figure 6. Average Nusselt number variation for smooth and v-corrugated SACs. (a) (p/H) = with different values of (e/H); (b) (p/H) = with different values of (e/H); (c) (p/H) = with different values of (e/H).

The average outlet air temperature is shown in Fig. 7 as a function of the *Re* for the chosen values of (*e/H*) and (*p/H*). The results demonstrate that, regardless of the shape of the absorber, the outlet temperature will decrease as the Reynold number rises. In addition, it is evident the average temperature of outlet air rises with height (*e/H*) for a given pitch (*p/H*) and Reynolds number as discussed above, and is generally higher than smooth because corrugated plates have the significant advantage of better solar radiation absorption than smooth ones, which improve the coefficients of heat transfer between the absorber and the flow of air. As compared to a smooth absorber plate SAC, which has an average temperature of 53 °C, a SAC of (*e/H* = 0.23 and *p/H* = 2) achieves a maximum average outlet temperature of roughly 61 °C.

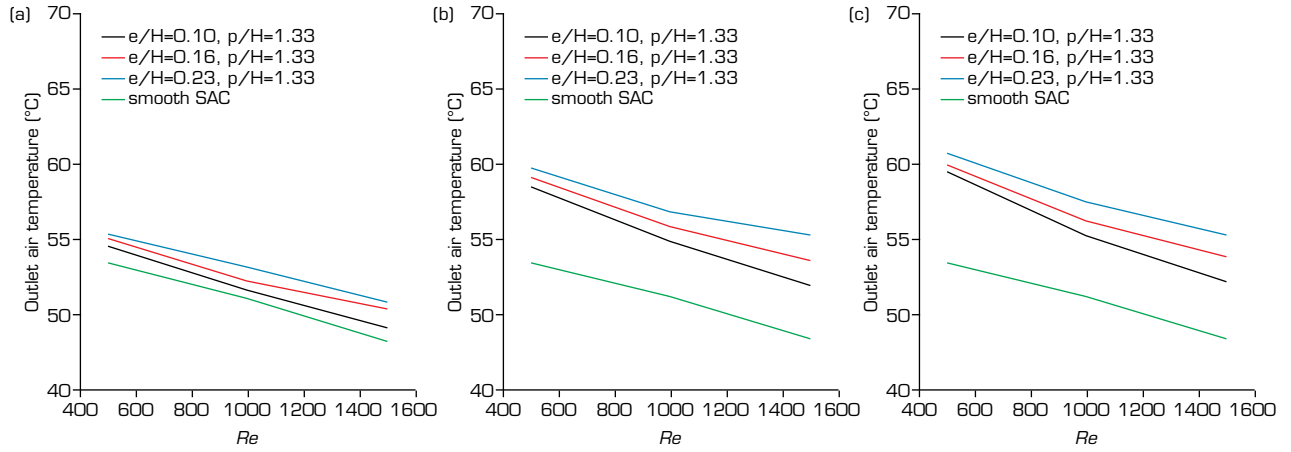

Source: Elaborated by the authors.

Figure 7. Variation of average temperature of outlet air for smooth and v-corrugated SACs at different values of height and pitch with Reynolds number. (a) (p/H) = 1.33 with different values of (e/H); (b) (p/H) = with different values of (e/H); (c) (p/H) = with different values of (e/H).

Friction Loss

One of the great challenges in designing a solar air collector is selecting the suitable parameters like average Nusselt number, average friction factor, and thermal performance of the collector components to achieve the best performance while keeping the lowest cost possible. Figure 8 displays the change of the average friction factor with *Re* at various heights (*e/H*) and pitches (*p/H*) for corrugated and smooth air collectors. In every situation, installing v-corrugation causes the average friction factor to be higher than in a smooth collector. The flow is obstructed by the corrugation. The results show that when the *Re* rises, the average *Cf* falls. Additionally, it is observed for a given value of the *Re* and (*p/H*), the average *Cf* increases dramatically as the (*e/H*) increases. It is brought on by the rise in flow route disruptions brought on by the rising value of (*e/H*). Additionally, it is observed that for fixed values of *Re* and height (*e/H*), the average *Cf* rises as (*p/H*) decreases. This is due to the fact that as pitch (*p/H*) drops, the number of corrugation zones grows and more flow blockage results.

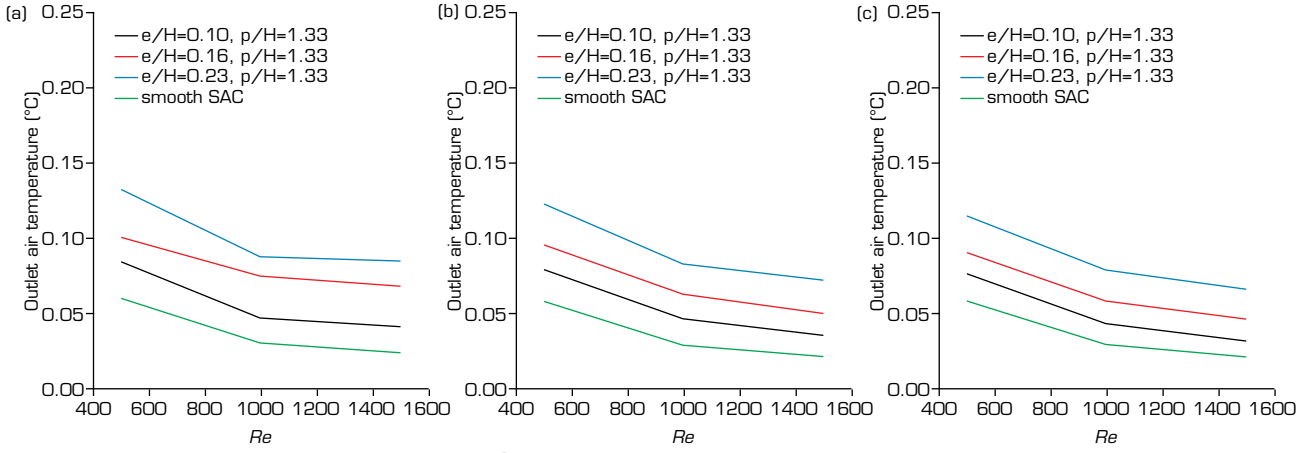

Source: Elaborated by the authors.

Figure 8. Variation of average friction factor for smooth SAC and v-corrugation SAC at distinct values of height and pitch with Reynolds number. (a) p/H) = 1.33 with different values of (e/H); (b) p/H) = with different values of (e/H); (c) p/H) = with different values of (e/H).

Thermal Efficiency

Figure 9 shows the influence of Reynolds number on the average thermal efficiency of the corrugated and smooth SAC during the simulated day. It is demonstrated that the thermal efficiency of the two SAC rises as Reynolds number increases, and that corrugated absorber plates have greater thermal efficiencies than smooth ones. It is discovered that, at a given value of the *Re* and (*p*/*H*), the average thermal efficiency increases dramatically as (*e*/*H*) increases. The highest thermal efficiency is seen for (*e*/*H* = 0.23), (*p*/*H* = 2), and is around 46.7%, as opposed to 33.1% for a smooth collector.

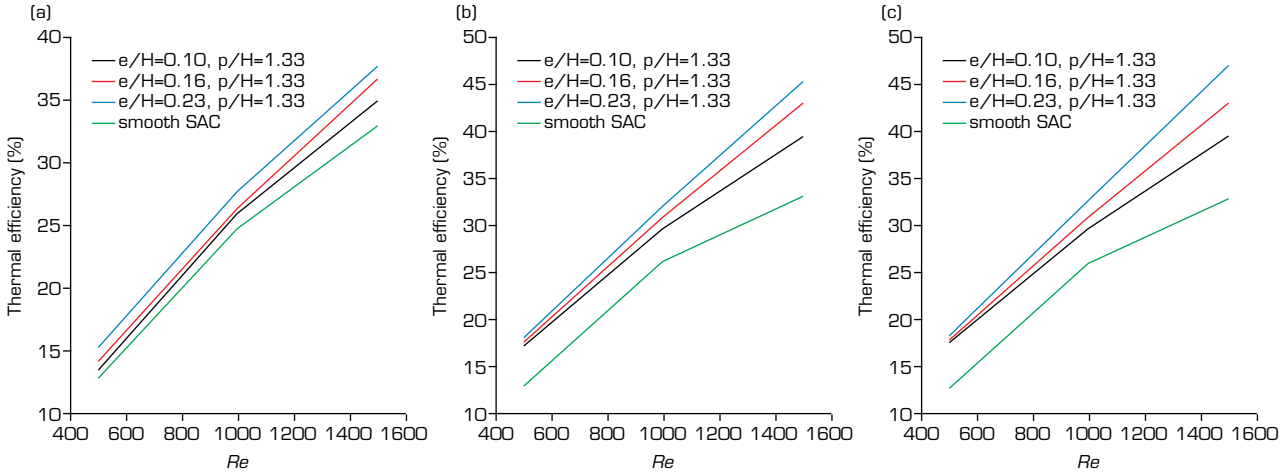

Source: Elaborated by the authors.

Figure 9. Variation of average thermal efficiency for smooth SAC and v-corrugation SAC at different values of height and pitch with Reynolds number. (a) (p/H) = 1.33 with different values of (e/H); (b) (p/H) = with different values of (e/H); (c) (p/H) = with different values of (e/H).

Thermohydraulic Performance Parameter (THPP)

Total performance of SACs, taking into account both an improvement in heat transmission and an increase in friction factor. Variation of THPP with Reynolds number is present in Fig. 10 for various heights (*e*/*H*) and pitches (*p*/*H*) for corrugated air collector. For a height (*e*/*H*) of 0.10, 0.16, and 0.23, the values of THPP ranged from 1.118 to 1.220, 1.079 to 1.161, and 1.058 to 1.157, respectively. In each case, the THPP values rised as the Reynolds number decreased. The results show that the values of THPP increased as the (*e*/*H*) decreased. Additionally, these values increased as the pitches (*p*/*H*) increased. Therefore, it can be said that for low *Re*, low (*e*/*H*), and higher (*p*/*H*), the v -corrugation in absorber plate SAC is more effective. In the range of parameters examined, greatest THPP value is 1.220 for (*e*/*H*) of 0.10, and (*p*/*H*) of 2, at a *Re* of 500.

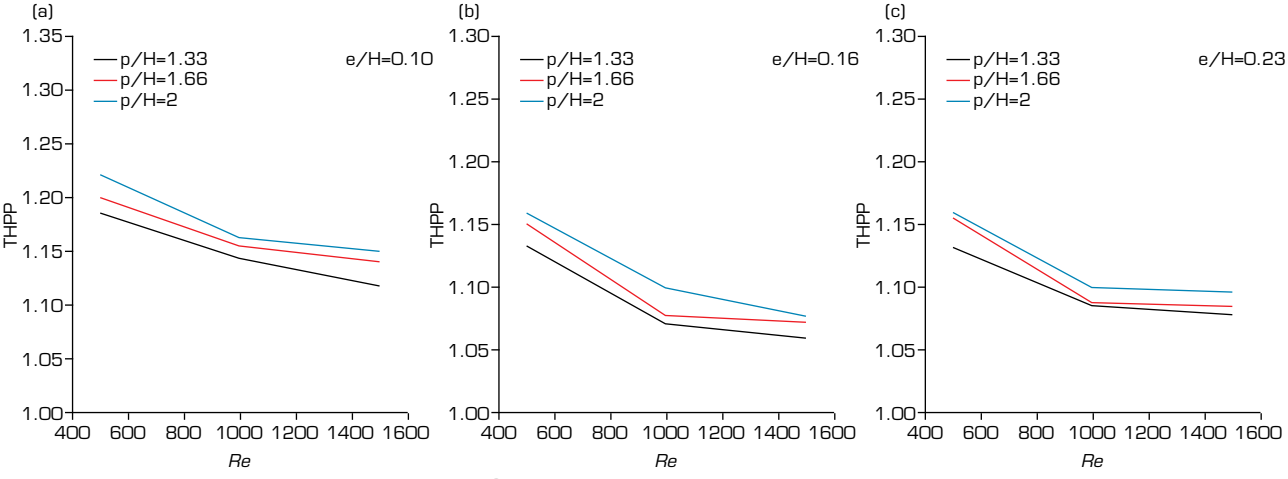

Source: Elaborated by the authors.

Figure 10. Variation of THPP for v-corrugation SAC at different values of height and pitch with Reynolds number. (a) (p/H) =1.33 with different values of (e/H); (b) (p/H) = with different values of (e/H); (c) (p/H) = with different values of (e/H).

CONCLUSIONS

The main findings of this investigation can be summarized as follows:

- The best ways to increase heat transfer rates from heated plates are observed to be v-corrugated roughened surfaces with varying height and pitch.
- The *Nu* and C_t are significantly influenced by the corrugation's parameters. It is obtained as *Re* grows, the C_t decreases while *Nu* increases.
- At a fixed value of (*p*/*H*) and *Re*, the average *Nu* and C_t rise when the height (*e*/*H*) increases, while they reduce as (*p*/*H*) rise.
- The highest average outlet temperature is found in the v-absorber SAC, where it is around 61 °C for a (*e*/*H* = 0.23 and *p*/*H* = 2) as opposed to 53 °C for the smooth absorber SAC.
- The thermal efficiency is at its highest level for a v-corrugation absorber SAC at (*e*/*H* = 0.23 and *p*/*H* = 2) and it is about 46.7% compared to 33.01% for smooth absorber SAC, which indicate the optimal configuration for a v-corrugation absorber SAC is at (*e*/*H*=0.23) and (*p*/*H*=2), verify a high performance.

CONFLICT OF INTEREST

Nothing to declare.

AUTHORS' CONTRIBUTIONS

Conceptualization: Abed AF; **Methodology:** Hamad RF; Abed AF; **Resources:** Hashim NAW; **Software:** Abed AF; **Data curation:** Hashim NAW; **Formal analysis:** Dahham RB; **Supervision:** Abed AF, Hamad RF; **Validation:** Dahham RB; **Preparation of original draft:** Hamad RF; **Writing:** Abed AF; **Proofreading and editing:** Hashim NAW.

DATA AVAILABILITY STATEMENT

Data sharing is not applicable.

FUNDING

Not applicable.

ACKNOWLEDGEMENTS

Not applicable.

REFERENCES

Aharwal KR, Gandhi BK, Saini JS (2008) Experimental investigation on heat transfer enhancement due to a gap in an inclined continuous rib arrangement in a rectangular duct of solar air heater. Renew Energ 33(4):585-596. https://doi.org/10.1016/j.renene.2007.03.023

Amraoui MA, Aliane K (2018) Three-dimensional analysis of air Flow in a flat plate solar collector. Period Polytech Mech Eng 62(2):126-135. https://doi.org/10.3311/PPme.11255

Chaichan MT, Abass KI, Al-Zubidi DS, Kazem HA (2016) Practical Investigation of Effectiveness of Direct Solar-Powered Air Heater. IJAEMS 2(7):1047-1053.

Chaube A, Sahoo PK, Solanki SC (2006) Analysis of heat transfer augmentation and flow characteristics due to rib roughness over absorber plate of a solar air heater. Renew Energ 31(3):317-331. https://doi.org/10.1016/j.renene.2005.01.012

Choi H-U, Choi K-H (2020) CFD Analysis on the Heat Transfer and Fluid Flow of Solar Air Heater having Transverse Triangular Block at the Bottom of Air Duct. Energies 13(5):1099. https://doi.org/10.3390/en13051099

Darici S, Kilic A (2020) Comparative study on the performances of solar air collectors with trapezoidal corrugated and flat absorber plates. Heat Mass Transfer 56(6):1833-1843. https://doi.org/10.1007/s00231-020-02815-y

Hakam M, Ichsani D, Suroso C (2016) Numerical investigation of heat transfer and fluid flow characteristic of V-corrugated plate solar air collector with prismatic fin as an extended surface. AIP Conf Proc 1778(1):030009. https://doi.org/10.1063/1.4965743

Hameed HG, Diabil HAN, Saeed MMA (2021) Performance of A New Model of Air Heating System: Experimental Investigation. J Mech Eng Res Dev 44(5):420-432.

Hassan HFA (2022) Experimental study and evaluation of single slope solar still combined with parabolic trough using nanofluid (Master's thesis). Najaf: Al-Furat Al-Awsat Technical University. In English. [accessed 2022 May 20]. https://cnj.atu.edu.iq/wp-content/uploads/2022/06/Hawraa-Fadhel-Abd-Hassan-2022-4-25.pdf

Hedayatizadeh M, Sarhaddi F, Safavinejad A, Ranjbar F, Chaji H (2016) Exergy loss-based efficiency optimization of a double-pass/glazed v-corrugated plate solar air heater. Energy 94:799-810. https://doi.org/10.1016/j.energy.2015.11.046

Karmare SV, Tikekar AN (2010) Analysis of fluid flow and heat transfer in a rib grit roughened surface solar air heater using CFD. Sol Energy 84(3):409-417. https://doi.org/10.1016/j.solener.2009.12.011

Kumar A, Gholap A, Gangarde R, Shinde SM, Vyavahare MP, Mete VB, Borude SA (2017) Performance Of Solar Air Heaters With Corrugated Absorber Plate- A CFD Approach. IJIRAS 4(11):76-86.

Manjunath MS, Karanth KV, Sharma NY (2018) Numerical investigation on heat transfer enhancement of solar air heater using sinusoidal corrugations on absorber plate. Int J Mech 138-139:219-228. https://doi.org/10.1016/j.ijmecsci.2018.01.037Naraghi MH, Blanchard S (2015) Twenty-four-hour simulation of solar chimneys. Energy Build 94:218-226. https://doi.org/10.1016/j.enbuild.2015.03.001

Promvonge P, Promthaisong P, Skullong S (2022) Heat transfer augmentation in solar heat exchanger duct with louver-punched V-baffles. Sol Energy 248:103-120. https://doi.org/10.1016/j.solener.2022.11.009

Rouissi W, Naili N, Jarray M, Hazami M (2021) CFD Numerical Investigation of a New Solar Flat Air-Collector Having Different Obstacles with Various Configurations and Arrangements. Math Probl Eng 2021:9991808. https://doi.org/10.1155/2021/9991808

Salih SM, Alsabery AI, Hussein AK, Ismael MA, Ghalambaz M, Hashim I (2023) Melting control of phase change material of semi-cylinders inside a horizontal baffled channel: Convective laminar fluid–structure interaction. J Energy Storage 58:106312. https://doi.org/10.1016/j.est.2022.106312

Varol Y, Oztop HF (2007) Buoyancy induced heat transfer and fluid flow inside a tilled wavy solar collector. Build Environ 42(5):2062-2071. https://doi.org/10.1016/j.buildenv.2006.03.001

Winbank WC (1963) Long-wave radiation from clear skies. Q J R Meteorol Soc 89(381):339-348. https://doi.org/10.1002/qj.49708938105

Yadav AS, Bhagoria JL (2013) Modeling and Simulation of Turbulent Flows through a Solar Air Heater Having Square-Sectioned Transverse Rib Roughness on the Absorber Plate. Sci World J 2013:827131. https://doi.org/10.1155/2013/827131

Zheng W, Zhang H, You S, Fu Y, Zheng X (2017) Thermal performance analysis of a metal corrugated packing solar air collector in cold regions. Appl Energy 203:938-947. https://doi.org/10.1016/j.apenergy.2017.06.01